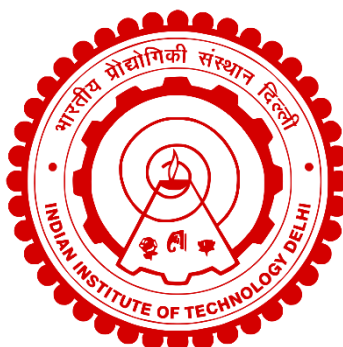


**CRYSTAL ENGINEERING OF LANTHANIDE BASED  
POLYOXOMOLYBDATES:  
THE TAXONOMY OF EXPLORING A STRUCTURAL  
LANDSCAPE**

**SHAILABH TEWARI**



**DEPARTMENT OF CHEMISTRY  
INDIAN INSTITUTE OF TECHNOLOGY DELHI  
JUNE 2023**

**© Indian Institute of Technology Delhi (IITD), New Delhi 2023**

**CRYSTAL ENGINEERING OF LANTHANIDE BASED  
POLYOXOMOLYBDATES: THE TAXONOMY OF  
EXPLORING A STRUCTURAL LANDSCAPE**

*by*

**SHAILABH TEWARI**

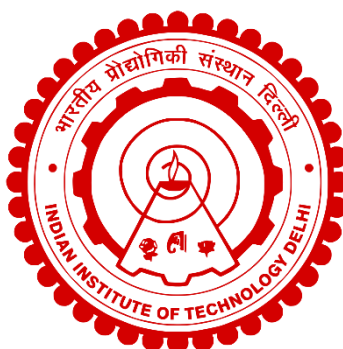
**DEPARTMENT OF CHEMISTRY**

*Submitted*

*In fulfillment of the requirements of the degree of*

**DOCTOR OF PHILOSOPHY**

*to the*



**INDIAN INSTITUTE OF TECHNOLOGY DELHI**

**JUNE 2023**

*Dedicated*  
*to*  
*my family and teachers*

## CERTIFICATE

This is to certify that the thesis entitled, “**Crystal Engineering of Lanthanide based Polyoxomolybdates: The Taxonomy of exploring a Structural Landscape**” being submitted by **Mr. Shailabh Tewari** to the Indian Institute of Technology Delhi for the award of the degree of **Doctor of Philosophy** in Chemistry, is a record of bonafide research work carried out by him. Mr. Shailabh Tewari has worked under my guidance and supervision and has fulfilled the requirements for the submission of this thesis, which to my knowledge has reached the requisite standard.

The results contained in this dissertation have not been submitted, in part or full, to any other university or institute for award of any degree or diploma.



(Supervisor)

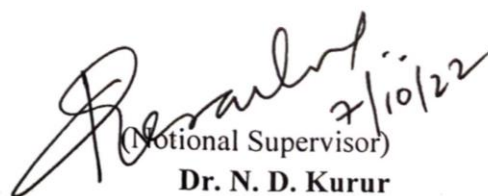
**Dr. A. RAMANAN**

Professor

Department of Chemistry

Indian Institute of Technology Delhi

New Delhi-110016



(Notional Supervisor)

**Dr. N. D. Kurur**

Professor

Department of Chemistry

Indian Institute of Technology Delhi

New Delhi-110016

## ACKNOWLEDGEMENTS

*First and foremost, I would like to offer my most sincere gratitude to my advisor, **Prof. Arunachalam Ramanan**, for his outstanding patience, boundless motivation, and extensive guidance. His guidance, co-operation and support were an integral part of my successful completion of the Ph.D. studies and the accompanying research. Without his guidance and support this thesis would not have taken this shape. His direction has shaped my understanding of the world as I see it. Under his tutelage I have aspired to be a better version of myself in a manner, unattainable any other way.*

*In addition to expressing my gratitude to my advisor, I would like to thank the members of the thesis committee: Prof. Ashok Kumar Ganguli, Prof. Neeraj Khare, and Prof. Pravin Ingole. The highly helpful recommendations and quick comments that they offered on my work turned out to be extremely profitable in terms of increasing the overall quality of the work. I wish to express my sincere thanks to the heads of the Department of Chemistry, Prof. Ravi Shankar, Prof. Anil J. Elias and Prof. N. D. Kurur for their valuable contribution and support throughout my Ph.D work at IIT Delhi. I would also like to thank all the staff associated with the Department of Chemistry, IIT Delhi.*

*I am highly obliged to Prof. G. Vijaya Prakash, Nanophotonics Lab, Department of Physics, Indian Institute of Technology Delhi, and members of his group, namely, Dr. Mohammed Adnan, Jitendra Nath Acharya, and others, for optical properties characterization as well as valuable inputs. I would also like to thank Dr. Sajesh P. Thomas for valuable discussion and support, Prof. J. J. Vittal, NUS, Singapore, and Dr. B. Sridhar, IICT, Hyderabad for their help in modelling crystal structures and Mr. Sami Makki, M/s. Matrix India for gifting native ruby crystals.*

*I would like to thank all my teachers through-out this academic journey for helping me throughout my studies and inspiring me to pursue my career in research. I would like to convey my heartfelt gratitude to my seniors Dr. Vineet Kumar, Dr. Balendra and Dr. Preethi Thomas, for teaching me various techniques and for becoming a wonderful advisor to ease my path in the whole journey. I would like to thank my colleagues, Dr. Bharti Singh, and Manisha Jadon for creating friendly atmosphere in the lab. I also thank my colleagues and friends who have stood by me through all the ups and downs in my life and continue to do so.*

*Finally, and most importantly, I would like to thank my family, I am grateful to my aunts and uncles for their constant support and encouragement and my brothers, sisters, nephews, and nieces for their faith in me. I deeply thank my source of inspiration: my parents, for their unwavering trust. Their support helped me overcome disappointments and their affection and support have boosted me throughout this journey.*

*My Ph.D thesis is dedicated to my teachers, family and friends.*

Shailabh Tewari

## ABSTRACT

The current state of art in synthetic materials chemistry lacks mechanistic understanding in terms of the formation of a crystal from soluble molecular species. This, thereby, creates a bottleneck in terms of designing synthesis of novel functional materials with desirable properties. The importance of retrosynthetic analysis via literature mining, in investigating the structural landscape of a set of molecular building blocks is highlighted. This approach facilitates the qualitative development of crystallization phase diagrams. Such techniques are necessary in absence of actual phase boundaries and phase equilibria, unattainable due to experimental limitations, to understand formation of a crystalline solid from soluble molecular species under given experimental condition. To be able to rationalize changes in crystal structures as a function of synthetic variables, a judicious choice of molecular building blocks is eminent such that the variations in their atomic connectivity must provide the compositional diversity to be able to assess the consequences of reaction variables on structure and in turn property. Thus, Polyoxomolybdates (POMos), were used as the primary building blocks in the study. These discrete anionic molecular analogues of bulk oxides were paired with lanthanide cations. The choice was eminent not only because of the multitude of applications envisaged for these multifunctional materials and the relative rarity such materials in the literature but also to understand the changes in the final crystal structures owing to the decreasing size of the lanthanide ions along the series. Among the POMo clusters, the Anderson-Evans cluster was chosen as the primary polyoxometalate anion in this study owing to its robustness and structural versatility as well as due to the fact that the hexamolybdo(VI)chromate(III) type of this cluster (i.e. with  $\text{Cr}^3$  as the heteroatom) is a molecular analogue of ruby. However, an earlier investigation from our group had reported the absence of emission from  $\text{Ln}^{3+}$  cations when coordinated with the Anderson-Evans cluster. To probe this further, we set out to investigate the structural landscape of ‘ $\text{Ln}^{3+}$ -Anderson-Evans<sup>-</sup>-sol’ system. In **Chapter II**, using a

systematic synthetic protocol, modified via literature analysis as well as experimental experience, we were able to isolate a series of solids where lanthanide-aquo complex was coordinated to the Anderson-Evans cluster (with both optically active  $\text{Cr}^{3+}$  and optically silent  $\text{Al}^{3+}$  as heteroatom). An interesting observation made during this study was that heavier lanthanides (heavier than  $\text{Ho}^{3+}$ ), due to their smaller size, preferred a slightly different crystal structure (**Series IIIb**) wherein a pair of octa-coordinated lanthanide hydrate complexes with a cluster and another anionic cluster balances the charge making the composition:  $[\text{Ln}(\text{H}_2\text{O})_7\{\text{X}(\text{OH})_6\text{Mo}_6\text{O}_{18}\}\text{Ln}(\text{H}_2\text{O})_7][\text{X}(\text{OH})_6\text{Mo}_6\text{O}_{18}]\cdot 16\text{H}_2\text{O}$  ( $\text{X}=\text{Cr}, \text{Al}$ ). Whereas lighter lanthanides that exhibited a nona-coordinated hydrated lanthanide cation coordinated to the cluster, forming a 1D-chain of composition:  $[\{\text{Ln}(\text{H}_2\text{O})_7\{\text{X}(\text{OH})_6\text{Mo}_6\text{O}_{18}\}\}]\cdot 4\text{H}_2\text{O}$  (**Series IIIa**). The similarity in the intermolecular interaction patterns made clear that the changes manifested in the structure of larger (La-Ho) and smaller (Er-Lu) lanthanides are due to the decrease in the size of the lanthanide cations. Photoluminescence (PL) of single crystals of all chromium molybdates including those with optically active  $\text{Sm}^{3+}$ ,  $\text{Eu}^{3+}$ ,  $\text{Tb}^{3+}$  and  $\text{Dy}^{3+}$  ions was dominated by a ruby-like emission in contrast to characteristic lanthanide emissions in corresponding aluminium analogues. Our results suggested a possible energy transfer from  $4f$  levels of lanthanide ions to  $3d$  levels of chromium(III), causing the quenching of lanthanide emission when it is coordinated with chromium molybdates. **Chapter III** describes the effect of changing the solvent used to solubilize lanthanide precursor from water to DMSO. The choice was dictated by its ligating nature, reasonable polarity, miscibility with water and a higher affinity for  $\text{Ln}^{3+}$  than water. Also, the number of Anderson-Evans based POMos with DMSO as part of the solid were only a handful. Furthermore, there was a need to isolate  $\text{Ln}^{3+}$  containing  $\text{Cr}^{3+}$ -Anderson-Evans cluster-based solids wherein lanthanide was not coordinated to the cluster. Our modified synthetic protocol resulted in the crystallization of two different concomitant series from the supramolecular aggregation of  $\{\text{Ln}(\text{DMSO})_4(\text{H}_2\text{O})_4\}$  and

$\{\text{Cr}(\text{OH})_6\text{Mo}_6\text{O}_{18}\}$ : (i) A 0D solid of the composition  $\{\text{Ln}(\text{DMSO})_4(\text{H}_2\text{O})_4\}\{\text{Cr}(\text{OH})_6\text{Mo}_6\text{O}_{18}\} \cdot \text{DMSO}$  (**Series IIIa**) where Ln=La, Ce and Pr and (ii) 1D chain of the composition,  $[\{\text{Ln}(\text{DMSO})_4\}\{\text{Cr}(\text{OH})_6\text{Mo}_6\text{O}_{18}\}] \cdot 2\text{DMSO} \cdot 2\text{H}_2\text{O}$  (**Series IIIb**) where Ln=La, Ce, Pr, Nd, Sm, Eu, Gd and Tb. Interestingly, in **Series IIIa**, the building block is a discrete lanthanide solvated POMo complex of 1:1 stoichiometry whereas in **Series IIIb**, lanthanide solvate is coordinated to the chromium molybdate cluster forming 1D chain. However, we succeeded in growing **Series IIIa** only with chromium-based cluster. **Chapter IV** reports the consequence of changing the solvent from DMSO to DMF along with the change of molybdenum source from  $\text{Na}_2\text{MoO}_4 \cdot 2\text{H}_2\text{O}$  to  $\text{K}_2\text{MoO}_4$ , which led to the isolation of another series of isostructural solids,  $\{\text{Ln}(\text{DMF})_4(\text{H}_2\text{O})_4\}\{\text{X}(\text{OH})_6\text{Mo}_6\text{O}_{18}\} \cdot y\text{H}_2\text{O}$  where X=Al, Cr (**Series IVb**). These 0D solids are significantly different from the 0D solids isolated in **Series IIIa**, where the complex  $\{\text{Ln}(\text{DMF})_4(\text{H}_2\text{O})_4\}^{3+}$  is not coordinated but interacts via H-bonding to the POMo cluster,  $\{\text{X}(\text{OH})_6\text{Mo}_6\text{O}_{18}\}^{3-}$ , as desired. As expected, PL of  $\text{Cr}^{3+}$  analogues showed emission from both optically active lanthanides as well as the chromium containing cluster. These results corroborated from our earlier observation and supported the hypothesis that absence of lanthanide emission in **Series IIa** resulted as a consequence of its coordination with the cluster providing a pathway for energy transfer from  $\text{Ln}^{3+}$  to  $\text{Cr}^{3+}$ . **Chapter V** reports the observation of a competing phase containing  $\beta$ -octamolybdate of the composition  $[\{\text{Ln}(\text{DMSO})_x(\text{H}_2\text{O})_y\}\{\text{NaMo}_8\text{O}_{26}\}]$  (**Series Va**) when DMSO was used as a solvent (**Chapter III**). Here, we report various  $\beta$ - $\text{Mo}_8\text{O}_{26}$  containing solids isolated when the heteroatoms  $\text{Cr}^{3+}$  or  $\text{Al}^{3+}$  were absent under our reaction condition. **Appendix A** details the effect of temperature under hydrothermal/solvothermal conditions, which led to the isolation of a series of solids with the composition  $[\{\text{Ln}(\text{H}_2\text{O})_{5-4}\}_2\{\text{Cr}(\text{OH})_6\text{Mo}_6\text{O}_{18}\}\{\text{LnMo}_{12}\text{O}_{42}\}] \cdot y\text{H}_2\text{O}$  (**Series A2**). The solid is built of two different POMo anions, namely, Anderson-Evans cluster,  $\{\text{Cr}(\text{OH})_6\text{Mo}_6\text{O}_{18}\}^{3-}$  and Dexter-Silverton cluster,  $\{\text{Ln}^{\text{III}}\text{Mo}_{12}\text{O}_{42}\}^{9-}$ . Solids of the **Series A2**

represent a rare class of POM based solids where two different POMo architectures are connected to each other through a pair of lanthanide complex via coordinate bonds, extending into a 1D chain. **Appendix B** reports the structure and characterization of two concomitant solids made of two different clusters, i.e., “extended octamolybdate”,  $\{\text{Mo}_8\text{O}_{27}\}^{6-}$ , and an “isopoly-Keggin”  $\{(\text{Mo}^{\text{VI}}_{12.5}\text{O}_{40})^{5-}$ , isolated in the presence of imidazole, a weak organic base. The observation of these two solids supported the idea that certain clusters tend to form in preference to the reaction medium – aqueous (reported in Inorganic Crystal Structure Database) or non-aqueous media/in presence of organic acid/bases (Reported in Crystal Structure Database), as evident in the databases.

Investigating the structural landscape of a set of molecular building blocks for correlation of structure with property has been the modus-operandi in materials synthesis. However, only a few studies focussed on the aspect of correlating synthesis with structure, which is vital in being able to design synthesis for targeted materials with desired properties. Hence, deliberate attempts were made such that there are minimal deviations in synthetic conditions among the various series of solids reported. In-situ generation of the POMo clusters from a one-pot synthesis was emphasized as it facilitated synthesis-structure-function correlation.

## सार

सिंथेटिक सामग्री रसायन विज्ञान में कला की वर्तमान स्थिति में घुलनशील आणविक प्रजातियों से क्रिस्टल के निर्माण के संदर्भ में यंत्रवत समझ का अभाव है। इस प्रकार, वांछनीय गुणों के साथ उपन्यास कार्यात्मक सामग्री के संश्लेषण को डिजाइन करने के मामले में यह एक बाधा उत्पन्न करता है। आणविक बिल्डिंग ब्लॉक्स के एक सेट के संरचनात्मक परिदृश्य की जांच में साहित्य खनन के माध्यम से रेट्रोसिंथेटिक विश्लेषण के महत्व पर प्रकाश डाला गया है। यह दृष्टिकोण क्रिस्टलीकरण चरण आरेखों के गुणात्मक विकास की सुविधा प्रदान करता है। ऐसी तकनीकें वास्तविक चरण सीमाओं और चरण संतुलन के अभाव में आवश्यक हैं, प्रयोगात्मक सीमाओं के कारण अप्राप्य, दी गई प्रयोगात्मक स्थिति के तहत घुलनशील आणविक प्रजातियों से क्रिस्टलीय ठोस पदार्थ के गठन को समझने के लिए। सिंथेटिक चर के एक समारोह के रूप में क्रिस्टल संरचनाओं में परिवर्तन को युक्तिसंगत बनाने में सक्षम होने के लिए, आणविक बिल्डिंग ब्लॉक्स के एक सेट का विवेकपूर्ण विकल्प इस तरह से प्रख्यात है कि उनकी परमाणु कनेक्टिविटी में भिन्नता प्रतिक्रिया के परिणामों का आकलन करने में सक्षम होने के लिए संरचनागत विविधता प्रदान करती है। संरचना और बदले में संपत्ति पर चर। इस प्रकार, पॉली-ओक्सो-मेटलतेस (POMos) का उपयोग अध्ययन में प्राथमिक बिल्डिंग ब्लॉक्स के रूप में किया गया था। बल्क ऑक्साइड के इन असतत आयनिक आणविक एनालॉग्स को लैथेनाइड उद्घरणों के साथ जोड़ा गया था। यह विकल्प न केवल बहु-कार्यात्मक सामग्रियों और साहित्य में ऐसी सामग्री की सापेक्ष दुर्लभता का उपयोग करने वाले अनुप्रयोगों की भीड़ के कारण प्रसिद्ध था, बल्कि श्रृंखला के साथ लैथेनाइड आयनों के घटते आकार के कारण अंतिम क्रिस्टल संरचनाओं में परिवर्तन को समझने के लिए भी था। पोमो समूहों के बीच, एंडरसन-इवांस क्लस्टर को इस अध्ययन में प्राथमिक पॉलीऑक्सोमेटलेट आयन के रूप में चुना गया था, इसकी मजबूती और संरचनात्मक बहुमुखी प्रतिभा के साथ-साथ इस तथ्य के कारण कि इस क्लस्टर के हेक्सामोलिब्डो (VI) क्रोमेट (III) प्रकार (यानी।  $Cr^{3+}$  हेटेरोएटम के रूप में) माणिक का एक आणविक एनालॉग है। हालाँकि, हमारे समूह की एक पहले की जाँच ने एंडरसन-इवांस क्लस्टर के साथ समन्वित होने पर  $Ln^{3+}$  उद्घरणों

के ल्यूमिनेसेंस के शमन की सूचना दी थी। इसकी और जांच करने के लिए, हम 'Ln<sup>3+</sup>- अन्देर्सन्-एवान्स-विलायक' प्रणाली के संरचनात्मक परिदृश्य की जांच करने के लिए निकल पड़े।

अध्याय II में, एक व्यवस्थित सिंथेटिक प्रोटोकॉल का उपयोग करते हुए, साहित्य विश्लेषण के साथ-साथ प्रयोगात्मक अनुभव के माध्यम से संशोधित, हम ठोस पदार्थों की एक सीरीज़ को अलग करने में सक्षम थे जहां लैंथेनाइड-एक्वा कॉम्प्लेक्स को एंडरसन-इवांस क्लस्टर (वैकल्पिक रूप से सक्रिय Cr<sup>3+</sup> और वैकल्पिक रूप से दोनों के साथ) के साथ समन्वयित किया गया था। मूक Al<sup>3+</sup> हेटेरोएटम के रूप में)। इस अध्ययन के दौरान किया गया एक दिलचस्प अवलोकन यह था कि भारी लैंथेनाइड्स, उनके छोटे आकार के कारण, थोड़ा अलग क्रिस्टल संरचना (सीरीज़ IIb) को पसंद करते थे, जिसमें लाइटर लैंथेनाइड्स की तुलना में ऑक्टा-समन्वित लैंथेनाइड हाइड्रेट कॉम्प्लेक्स की एक जोड़ी 1D-श्रृंखला (सीरीज़ IIa) प्रदर्शित करती थी। हालांकि, इंटरमॉलिक्युलर इंटरैक्शन पैटर्न में समानता ने स्पष्ट किया कि बड़े (La-Ho) और छोटे (Er-Lu) लैंथेनाइड्स की संरचना में प्रकट परिवर्तन लैंथेनाइड के आकार में कमी के कारण हैं। ऑप्टिकल रूप से सक्रिय Sm<sup>3+</sup>, Eu<sup>3+</sup>, Tb<sup>3+</sup> और Dy<sup>3+</sup> आयनों सहित सभी क्रोमियम मोलिब्डेट्स के एकल क्रिस्टल की फोटोल्यूमिनेसेंस (PL) संबंधित एल्यूमीनियम एनालॉग्स में विशेषता लैंथेनाइड उत्सर्जन के विपरीत रूबी जैसे उत्सर्जन का प्रभुत्व था। हमारे परिणामों ने लैंथेनाइड आयनों के 4f स्तरों से क्रोमियम (III) के 3d स्तरों तक एक संभावित ऊर्जा हस्तांतरण का सुझाव दिया, जिससे क्रोमियम मोलिब्डेट्स के साथ समन्वयित होने पर लैंथेनाइड उत्सर्जन का शमन होता है। अध्याय III लैंथेनाइड अग्रदूत को पानी से डीएमएसओ में घोलने के लिए उपयोग किए जाने वाले विलायक को बदलने के प्रभाव का वर्णन करता है। पसंद इसकी बंधन प्रकृति, उचित ध्रुवता, पानी के साथ गलतता और पानी की तुलना में Ln<sup>3+</sup> के लिए एक उच्च आत्मीयता द्वारा निर्धारित किया गया था। इसके अलावा, ठोस पदार्थ के हिस्से के रूप में डीएमएसओ के साथ एंडरसन-इवांस आधारित पोमो की संख्या केवल एक मुट्ठी भर थी। Ln<sup>3+</sup> को Cr<sup>3+</sup>-एंडरसन-इवांस क्लस्टर-आधारित ठोस पदार्थों से अलग करने की आवश्यकता थी, जिसमें लैंथेनाइड को क्लस्टर में समन्वित नहीं किया गया था। हमारे संशोधित सिंथेटिक प्रोटोकॉल के

परिणामस्वरूप  $\{Ln(DMSO)_4(H_2O)_4\}$  और  $\{Cr(OH)_6Mo_6O_{18}\}$  के सुपरमॉलेक्यूलर एकत्रीकरण से दो अलग-अलग सहवर्ती सीरीज़ का क्रिस्टलीकरण हुआ: (i) संरचना का एक 0D ठोस पदार्थ  $\{Ln(DMSO)_4(H_2O)_4\}\{Cr(OH)_6Mo_6O_{18}\} \cdot DMSO$  (श IIIa) जहां  $Ln=La, Ce$  और  $Pr$  और (ii) संरचना की 1D श्रृंखला,  $[\{Ln(DMSO)_4\}\{Cr(OH)_6Mo_6O_{18}\}] \cdot 2DMSO \cdot 2H_2O$  (सीरीज़ IIIb) जहां  $Ln=La, Ce, Pr, Nd, Sm, Eu, Gd$  और  $Tb$ ।

दिलचस्प बात यह है कि सीरीज़ IIIa में, बिलिंग ब्लॉक 1:1 स्टोइकोमेट्री का एक असतत लैंथेनाइड सॉल्वेटेड पोमो कॉम्प्लेक्स है, जबकि सीरीज़ IIIb में, लैंथेनाइड सॉल्वेट को 1D चेन बनाने वाले क्रोमियम मोलिब्डेट क्लस्टर से समन्वित किया जाता है। हालांकि, हम सीरीज़ IIIb को केवल एल्यूमीनियम-आधारित क्लस्टर के साथ विकसित करने में सफल रहे। अध्याय IV, सॉल्वेंट को DMSO से DMF में बदलने के साथ-साथ  $Na_2MoO_4 \cdot 2H_2O$  से  $K_2MoO_4$  में मोलिब्डेनम स्रोत के परिवर्तन की रिपोर्ट करता है, जिसके कारण आइसोस्ट्रक्चरल सॉलिड की एक और सीरीज़ का अलगाव हुआ,  $\{Ln(DMF)_4(H_2O)_4\}\{X(OH)_6Mo_6O_{18}\} \cdot yH_2O$  जहां  $X=Al, Cr$  (सीरीज़ IVb)। ये 0डी सॉलिड सीरीज़ IIIa से काफी अलग हैं, जहां कॉम्प्लेक्स,  $\{Ln(DMF)_4(H_2O)_4\}^{3+}$  को ऑर्डिनेटेड नहीं है, लेकिन POMo क्लस्टर के लिए H-बॉन्ड है,  $\{X(OH)_6Mo_6O_{18}\}^{3-}$  इच्छानुसार। जैसा कि अपेक्षित था,  $Cr^{3+}$  एनालॉग्स के PL ने वैकल्पिक रूप से सक्रिय लैंथेनाइड्स के साथ-साथ क्रोमियम युक्त क्लस्टर दोनों से उत्सर्जन दिखाया। इन परिणामों ने हमारे पहले के अवलोकन से पुष्टि की और इस परिकल्पना का समर्थन किया कि लैंथेनाइड ल्यूमिनेसेंस के शमन का परिणाम क्लस्टर के साथ इसके समन्वय के परिणामस्वरूप  $Ln^{3+}$  से  $Cr^{3+}$  तक ऊर्जा हस्तांतरण के लिए मार्ग प्रदान करना है। अध्याय V एक प्रतिस्पर्धी चरण के अवलोकन की रिपोर्ट करता है जिसमें संरचना के  $\beta$ -ऑक्टा मोलिब्डेट  $[\{Ln(DMSO)_x(H_2O)_y\}\{NaMo_8O_{26}\}]$  (सीरीज़ Va) शामिल हैं, जब DMSO को विलायक (अध्याय III) के रूप में इस्तेमाल किया गया था। यहां, हम विभिन्न  $\beta$ -ऑक्टा मोलिब्डेट की रिपोर्ट करते हैं जिसमें अलग-थलग ठोस पदार्थ होते हैं जब हेटेरोएटम  $Cr^{3+}$  या  $Al^{3+}$  हमारी प्रतिक्रिया की स्थिति में अनुपस्थित थे। परिशिष्ट ए में हाइड्रोथर्मल/सॉल्वोथर्मल

स्थितियों के तहत तापमान के प्रभाव का विवरण दिया गया है, जिसके कारण संरचना के साथ ठोस पदार्थों की एक श्रृंखला का अलगाव हुआ  $[\{\text{Ln}(\text{H}_2\text{O})_4\}_2\{\text{Cr}(\text{OH})_6\text{Mo}_6\text{O}_{18}\}\{\text{LnMo}_{12}\text{O}_{42}\}].y\text{H}_2\text{O}$  (सीरीज़ ए2)। ठोस पदार्थ दो अलग-अलग पोमो आयनों से बना है, अर्थात् एंडरसन-इवांस क्लस्टर,  $\{\text{Cr}(\text{OH})_6\text{Mo}_6\text{O}_{18}\}^{3-}$  और डेक्सटर-सिल्वरटन क्लस्टर,  $\{\text{Ln}^{\text{III}}\text{Mo}_{12}\text{O}_{42}\}^9-$ । सीरीज़ A2 के ठोस पीओएम आधारित ठोस पदार्थों के एक दुर्लभ वर्ग का प्रतिनिधित्व करते हैं जहां दो अलग-अलग पोमो आर्किटेक्चर एक दूसरे से समन्वय बांड के माध्यम से लैथेनाइड कॉम्प्लेक्स की एक जोड़ी के माध्यम से जुड़े होते हैं, जो 1 डी श्रृंखला में विस्तारित होते हैं। परिशिष्ट बी दो अलग-अलग समूहों से बने दो सहवर्ती ठोसों की संरचना और लक्षण वर्णन की रिपोर्ट करता है, अर्थात्, "विस्तारित-ऑक्टाहोमोलिब्डेट",  $\{\text{Mo}_8\text{O}_{27}\}^{6-}$ , और एक "आइसोपॉली-केगिन"  $\{(\text{Mo}^{\text{VI}}_{12.5}\text{O}_{40})\}^{5-}$ , अलग-अलग में इमिडाज़ोल की उपस्थिति, एक कमजोर कार्बनिक आधार। इन दो ठोस पदार्थों के अवलोकन ने इस विचार का समर्थन किया कि कुछ क्लस्टर प्रतिक्रिया माध्यम - जलीय या गैर-जलीय मीडिया की वरीयता में बनते हैं, जैसा कि क्रिस्टल संरचना डेटाबेस में स्पष्ट है।

संपत्ति के साथ संरचना के सहसंबंध के लिए आणविक बिल्डिंग ब्लॉक्स के एक सेट के संरचनात्मक परिदृश्य की जांच करना सामग्री संश्लेषण में तौर-तरीका रहा है। हालांकि, केवल कुछ अध्ययनों ने संरचना के साथ सहसंबद्ध संश्लेषण के पहलू पर ध्यान केंद्रित किया, जो वांछित गुणों के साथ लक्षित सामग्री के लिए संश्लेषण को डिजाइन करने में सक्षम होने में महत्वपूर्ण है। इसलिए, जानबूझकर प्रयास किए गए थे कि रिपोर्ट किए गए ठोस पदार्थों की विभिन्न श्रृंखलाओं के बीच सिंथेटिक स्थितियों में न्यूनतम विचलन हो। एक पॉट संश्लेषण से पोमो समूहों की इन-सीटू पीढ़ी पर जोर दिया गया था क्योंकि यह संश्लेषण-संरचना-कार्य सहसंबंध की सुविधा प्रदान करता था।

## TABLE OF CONTENTS

CERTIFICATE.....	i
ACKNOWLEDGEMENTS.....	ii
ABSTRACT.....	iv
LIST OF CONTENT.....	xii
LIST OF FIGURES.....	xvii
LIST OF TABLES.....	xxv
ABBREVIATIONS.....	xxviii
<b>Chapter I: Introduction .....</b>	<b>1</b>
<b>I.1 Introduction .....</b>	<b>2</b>
<b>I.2 Challenges in Crystal Engineering of functional materials.....</b>	<b>2</b>
<b>I.3 The ‘Retrosynthetic’ approach .....</b>	<b>3</b>
<b>I.4 Why Polyoxomolybdates (POMos)? .....</b>	<b>6</b>
<b>I.5 Nucleation of POMo cluster-based solids in aqueous medium .....</b>	<b>7</b>
<b>I.6 Structural determinants for the formation of POMo clusters .....</b>	<b>8</b>
I.6.1 pH of the reaction medium and concentration of reactants .....	8
I.6.2 Temperature under hydrothermal/solvothermal conditions .....	8
I.6.3 Choice of solution media.....	9
I.6.4 Nature of organic ligands .....	9
<b>I.7 Choice of POMo cluster: Anderson-Evans cluster.....</b>	<b>10</b>
I.7.1 Photoluminescence of $\{\text{Cr}(\text{OH})_6\text{Mo}_6\text{O}_{18}\}^{3-}$ : Tunable inorganic molecular Ruby .....	14
<b>I.8 Motivation for the present work .....</b>	<b>19</b>

<b>Chapter II: Photoluminescence properties of two closely related isostructural series based on Anderson-Evans cluster coordinated with lanthanides [Ln(H<sub>2</sub>O)<sub>7</sub>{X(OH)<sub>6</sub>Mo<sub>6</sub>O<sub>18</sub>}]·yH<sub>2</sub>O, X=Al, Cr.....</b>	<b>38</b>
<b>II.1 Introduction.....</b>	<b>40</b>
<b>II.2 Experimental Section.....</b>	<b>41</b>
II.2.1 Modified synthetic protocol: .....	43
II.2.2 Crystal structures .....	44
<b>II.2.3. Crystallization of lanthanide coordinated chromium/aluminum hexamolybdates .....</b>	<b>55</b>
<b>II.3 Excitation and Emission spectra of rare-earth chromium/ aluminum molybdates .</b>	<b>56</b>
<b>II.4 Physical Measurements .....</b>	<b>70</b>
II.4.1 Single-crystal X-ray diffraction .....	70
II.4.2 Powder X-ray diffraction .....	70
II.4.3 Optical measurements .....	73
II.4.4 Vibrational Spectroscopy .....	74
II.4.5 Thermal Studies.....	80
<b>II.5 Summary.....</b>	<b>86</b>
<b>Chapter III: Synthesis and Characterization of Two Concomitant Series Based on Anderson-Evans Cluster Coordinated with Lanthanides in Water/DMSO Binary Solution. ....</b>	<b>92</b>
<b>III.1 Introduction .....</b>	<b>94</b>
III.1.1 Choice of DMSO .....	95
III.1.2 Literature Analysis.....	96

<b>III.2 Synthetic protocol:</b> .....	<b>98</b>
<b>III.3 Physical Measurements</b> .....	<b>107</b>
III.3.1 Single-crystal X-ray diffraction .....	107
III.3.2 Powder X-ray diffraction .....	107
III.3.3 Vibrational Spectroscopy.....	112
III.3.4 Thermal Studies .....	118
<b>Chapter IV: Synthesis, Characterization and Photoluminescent Properties of a Series of Lanthanide Containing Anderson-Evans Cluster-Based Solids Where the Cluster is Not Coordinated to the Ln<sup>3+</sup> Moiety.</b> .....	<b>125</b>
<b>IV.1 Introduction</b> .....	<b>127</b>
IV.1.1 Database Analysis DMF containing Chromium-molybdates .....	127
<b>IV.2 Synthetic protocol</b> .....	<b>128</b>
<b>IV.3 Crystal Structures</b> .....	<b>129</b>
<b>IV.4 Photoluminescence Studies</b> .....	<b>132</b>
<b>IV.5 Physical Measurements</b> .....	<b>137</b>
IV.5.1 Single-crystal X-ray diffraction.....	137
IV.5.2 Powder X-ray diffraction.....	138
IV.5.3 Optical Measurements .....	143
IV.5.4 Vibrational Spectroscopy.....	144
IV.5.5 Thermogravimetric Analysis .....	146
<b>IV.6 Summary</b> .....	<b>146</b>

<b>Chapter V: Structural Variation and Characterization of <math>\beta</math>-octamolybdate Containing Phases as a Function of Solvent and Molybdenum Source, in the Absence of <math>\text{Cr}^{3+}</math> or <math>\text{Al}^{3+}</math>.....</b>	<b>151</b>
<b>V.1 Introduction.....</b>	<b>153</b>
<b>V.2 Synthetic Protocol .....</b>	<b>156</b>
<b>V.3 Structural chemistry of <math>\beta</math>-<math>\{\text{Mo}_8\text{O}_{26}\}</math> based solids.....</b>	<b>158</b>
<b>V.4 Crystal Structures .....</b>	<b>159</b>
<b>V.5 Physical Measurements .....</b>	<b>181</b>
V.5.1 Single-crystal X-ray diffraction .....	181
V.5.2 Powder X-ray diffraction .....	181
V.5.3 Vibrational Spectroscopy .....	190
<b>V.6 Summary.....</b>	<b>201</b>
<b>Appendix A: Synthesis and characterization of a series of solids containing two POMo clusters coordinated via a pair of lanthanide hydrates, under hydrothermal condition. ....</b>	<b>204</b>
<b>A.1 Introduction.....</b>	<b>206</b>
<b>A.2 Synthetic Protocol .....</b>	<b>207</b>
<b>A.3 Crystal Structures .....</b>	<b>208</b>
<b>A.4 Summary.....</b>	<b>216</b>
<b>Appendix B: Synthesis and Characterization of Concomitantly Crystallized Extended Octamolybdate <math>\{\text{Mo}_8\text{O}_{27}\}^{6-}</math> and Isopoly-Keggin <math>\{(\text{Mo}^{\text{VI}}_{0.5}\text{O}_4)\text{Mo}_{12}\text{O}_{36}\}^{5-}</math> Based Solids.....</b>	<b>217</b>

<b>B.1 Introduction .....</b>	<b>219</b>
<b>B.2 Synthetic Protocol .....</b>	<b>220</b>
<b>B.3 Crystal Structures .....</b>	<b>221</b>
<b>B.4 Summary .....</b>	<b>225</b>
<b>Chapter VI: Summary Conclusions and Future Directions.....</b>	<b>228</b>
<b>VI.1 Summary .....</b>	<b>228</b>
<b>VI.2 Conclusions .....</b>	<b>232</b>
<b>VI.3 Future Directions.....</b>	<b>233</b>
<b>Appendix C: Literature Survey of <math>\{\text{Cr}(\text{OH})_y\text{Mo}_6\text{O}_{18}\}^{(9-y)-}</math> based solids reported in Crystal Structure Database v5.43.....</b>	<b>237</b>
<b>Hyperlink for Crystallographic Information Files (CIF).....</b>	<b>260</b>
<b>Academic Resume of the Author.....</b>	<b>261</b>

## LIST OF FIGURES

- Fig. I.1** A diagrammatic description of the modus-operandi of retrosynthetic analysis in exploring a structural landscape. The understanding of crystallization in terms of soluble molecular analogues facilitates subsequent synthetic attempts in order to realise targeted solids. ....5
- Fig. I.2** The speciation of  $\{\text{MoO}_4\}^{2-}$  species in aqueous solution. In intermediate pH range, leading to multitude of POMo architectures via a series of hydrolysis and condensation steps. ....7
- Fig. I.3** The Anderson-Evans cluster, named after J. S. Anderson and H. T. Evans (left). The disc shaped cluster consists of edge shared octahedra such that the central cavity nests a multitude of heteroatoms (right). ....10
- Fig. I.4** An analysis of Anderson-Evans cluster-based solids over the last decade with different heteroatoms using CSD version 5.43 (updated June 2022). ....12
- Fig. I.5** A CSD 5.43 (updated June 2022) analysis of hybrid solids reported with Anderson-Evans cluster with different heteroatoms and common ligands. Notice that the most common ligands are weak acids/bases. ....12
- Fig. I.6** The structural versatility in Anderson-Evans cluster-based solids. ....13
- Fig. I.7** Synthesis- -Structure-Property correlation leading to multiple applications in.....14
- $\{\text{M}(\text{sol})\}^{n+}-\{\text{X}(\text{OH})_y\text{Mo}_6\text{O}_{18}\}^{m-}$ -Org system. ....14
- Fig. I.9** (a)  $\text{Ln}^{3+}$  containing  $\{\text{Cr}(\text{OH})_6\text{Mo}_6\text{O}_{18}\}^{3-}$  cluster-based solids reported by our group. The luminescence of selected solids exhibiting the emission like ruby. (b) Schematic energy level scheme for  $\text{Cr}^{3+}$  ion depicting possible internal processes (blue and red colors indicate the absorption and emission transition/levels respectively. Broad green color arrow indicates the laser excitation). ....16

**Fig. II.1** The modified synthetic protocol led to the isolation of Series IIa for lighter lanthanides, till  $\text{Ho}^{3+}$ , and Series IIb for heavier lanthanides, for both  $\text{Cr}^{3+}$  as well as  $\text{Al}^{3+}$  as heteroatom. The red arrows depict the solids being reported for the first time. Luminescent lanthanides are depicted in coloured circles. Figure also shows optical images of both single crystal and polycrystalline form of each member.....**44**

**Fig. II.2** (a) The building block in Series IIa,  $[\text{Tb}(\text{OH}_2)_7\{\text{Al}(\text{OH})_6\text{Mo}_6\text{O}_{18}\}]\cdot 4\text{H}_2\text{O}$  (b) The nine-coordinated Tb coordinates with the cluster oxygens O24 and O20 extending into 1D chains. Coordination of lanthanide with terminal oxygens of the cluster at 1,3 position w.r.t. Mo atoms forming the hexagonal ring. Adjacent chains interact through  $\text{O}_{\text{Mo}}-\text{H}\cdots\text{O}_{\text{w}}$ . Lattice water molecules also facilitate H-bonding interactions. ....**49**

**Fig. II.3** Powder X-ray diffraction patterns of Series IIa,  $[\text{Ln}(\text{OH}_2)_7\{\text{X}(\text{OH})_6\text{Mo}_6\text{O}_{18}\}]\cdot 4\text{H}_2\text{O}$ ,  $\text{Ln}=\text{Y, La, Ce, Pr, Nd, Sm, Eu, Gd, Tb, Dy}$  and  $\text{Ho}$  and Series IIb,  $[(\text{H}_2\text{O})_7\text{Ln}\{\text{M}(\text{OH})_6\text{Mo}_6\text{O}_{18}\}\text{Ln}(\text{OH}_2)_7]\{\text{M}(\text{OH})_6\text{Mo}_6\text{O}_{18}\}\cdot 16\text{H}_2\text{O}$ ,  $\text{Ln}=\text{Er, Tm}$  and  $\text{Yb}$ .  $\{\text{X}=\text{Cr}(\text{left}), \text{Al}(\text{right})\}$ . ....**51**

**Fig. II.4** (a)The complex cation,  $[(\text{H}_2\text{O})_7\text{Tm}\{\text{Al}(\text{OH})_6\text{Mo}_6\text{O}_{18}\}\text{Tm}(\text{OH}_2)_7]^{3+}$  and the cluster anion  $\{\text{Al}(\text{OH})_6\text{Mo}_6\text{O}_{18}\}^{3-}$  are the building blocks in Series IIb along with 16 lattice water molecules. (b) The ions aggregate through H-bonding interactions. Series IIb is an example of a molecular solid (0D). The anionic Anderson-Evans cluster is depicted in orange for clarity. ....**51**

**Fig. II.5** (a) Stacking of 1D zig-zag chains on ab plane and (b) 1D chains stabilized through  $\text{O}_{\text{Mo}}-\text{H}\cdots\text{O}_{\text{w}}$  in Series IIa. (c) Growth of 0D molecular solid on ab-plane. Apart from electrostatic interaction, the lanthanide complex derivatised by the cluster,  $[(\text{H}_2\text{O})_7\text{Tm}\{\text{Al}(\text{OH})_6\text{Mo}_6\text{O}_{18}\}\text{Tm}(\text{OH}_2)_7]^{3+}$  and the anionic cluster,  $\{\text{Al}(\text{OH})_6\text{Mo}_6\text{O}_{18}\}$  also interact through  $\text{O}_{\text{Mo}}-\text{H}\cdots\text{O}_{\text{w}}$ . Notice the strikingly similar H-bonding pattern on ab plane in

(b) Series IIa and (d) Series IIb. In (c) and (d), the anionic clusters are depicted in orange. The water molecules coordinated to lanthanide cations are omitted for clarity. ....54

**Fig. II.6** (a) 1D chains along [010] and its projection on bc plane in Series IIa. (b) The discontinuous arrangement of cations and anions in Series IIb stacked one over the other closely resemble Series IIa. The discrete anionic Anderson-Evans cluster is depicted in orange for clarity.....55

**Fig. II.7** The Emission spectra of single crystals of (a)  $[\text{Ln}(\text{OH}_2)_7\{\text{Cr}(\text{OH})_6\text{Mo}_6\text{O}_{18}\}]\cdot y\text{H}_2\text{O}$ , and (b)  $[\text{Ln}(\text{OH}_2)_7\{\text{Al}(\text{OH})_6\text{Mo}_6\text{O}_{18}\}]\cdot y\text{H}_2\text{O}$ . Ln= Sm, Eu, Tb, Dy and Tm. The Bright field (BF) and PL images (PL) are given at left and right sides for respective crystals. PL spectra and images are recorded using 400nm laser excitation coupled to a microscope. \*Excited by 380nm of Xe lamp coupled to a monochromator (see text).....58

**Fig. II.8** The emission spectra of infrared rare-earth containing Chromium molybdate complexes. The corresponding bright field (BF) and Photoluminescence (PL) images are shown (leftside of each emission spectra). Excited by 400nm diode laser (see text).....59

**Fig. II.10** (a) The relative emission spectra comparison between EuAl<sub>2</sub>1, EuCr<sub>7</sub> and naturally occurring Ruby recorded under similar conditions (Excited by 400nm diode laser, ~ 10mW). Corresponding PL images are shown in the inset. (b)Emission spectra of EuAl<sub>2</sub>1 and EuCr<sub>7</sub> along with the schematic representation of emission mechanism for either energy transfer between lanthanide and lower lying Cr<sup>3+</sup>energy levels (EuCr<sub>7</sub>) or within the Eu<sup>3+</sup> ion energy levels (EuAl<sub>2</sub>1). ....62

**Fig. II.11** The emission spectra of TbAl<sub>2</sub>3 at various excitations. Excitation spectra monitored at 543nm is also given at the top (gray color). The emission spectra when excited at 400 nm gives no emission characteristics as evident from the excitation spectra that there is no absorption energy level at this excitation. The excitation source is a Xe lamp coupled to a monochromator (see text). ....64

<b>Fig. II.12</b> The emission spectra of TmCr13 and TmAl27 when excited at 400 nm diode laser. TmAl27 shows very low emission in UV-violet region, along with the substrate emission (marked in the gray shaded area). The corresponding bright field (BF) and PL images are also shown. ....	<b>65</b>
<b>Fig. II.13</b> Emission spectra of EuCr7 and NdCr5 and their corresponding PL images. The spectra are recorded under similar experimental condition (excited by 400nm diode laser, ~ 10mW) and the intensity of NdCr5 is about 4.6% with respect to EuCr7. ....	<b>65</b>
<b>Fig. II.14</b> Rietveld refinement plot for all the new solids reported in the work. The blue corresponds to the experimental data while the red represents calculated profile. ....	<b>71</b>
<b>Fig. II.15</b> (a-x) FT-IR spectra of all the solids recorded with Nicolet 5DX spectrometer. ....	<b>78</b>
<b>Fig. II.16</b> (a-d) FT-IR for solids recorded with Nicolet 6700 spectrometer. ....	<b>79</b>
<b>Fig. II.17</b> Thermal Analysis plots for (a)DyCr10, (b)HoCr11, (c)ErCr12, (d)TmCr13, (e)YbCr14, (f)PrAl18, (g)NdAl19, (h)TbAl23, (i)DyAl24, (j)ErAl26, (k) TmAl27 and (l) YbAl28. In most of the samples, artifacts like mass gain are observed above 500°C. Several factors like buoyancy effects, chemical reactions leading to the formation of hardly volatile compounds and adsorption of gaseous substances onto the sample could have caused a fluctuation in the mass. ....	<b>83</b>
<b>Fig. III.1</b> Molecular dimensions of DMSO compared to water [8]. ....	<b>95</b>
<b>Fig. III.2</b> Anderson-Evans cluster-based solids with DMSO in the Crystal Structure Database (CSD version 5.43 (November 2021)). ....	<b>96</b>
<b>Fig. III.3</b> Modified synthetic protocol leading to agglomerates of needle shaped Series IIIa and block shaped Series IIIb. ....	<b>99</b>
<b>Fig. III.4</b> The building block in Series IIIa, $\{\text{Ln}(\text{DMSO})_4(\text{H}_2\text{O})_4\{\text{Cr}(\text{OH})_6\text{Mo}_6\text{O}_{18}\}\cdot\text{DMSO}$ . Hydrogen atoms are omitted due to clarity. ....	<b>100</b>

<b>Fig. III.5 (a)</b> The growth of 1:1 complex of Series IIIa via a hydrogen bonded network between the stacks of clusters as well as (b) with the water molecules coordinated to lanthanide cations on the adjacent complexes. The lattice DMSO is represented in orange and the hydrogen atoms are omitted due to clarity. ....	<b>100</b>
<b>Fig. III.6</b> The building block in Series IIIb, $\{\text{Ln}(\text{DMSO})_4\{\text{Cr}(\text{OH})_6\text{Mo}_6\text{O}_{18}\}\cdot 2\text{DMSO}\cdot 3\text{H}_2\text{O}$ . Lattice solvent molecules and hydrogen atoms are omitted due to clarity. ....	<b>101</b>
<b>Fig. III.7</b> The growth of 1D chains in Series IIIb via a network of hydrogen bonds facilitated by lattice solvent molecules. ....	<b>101</b>
<b>Fig. III.8</b> The growth of 1:1 complex in Series IIIa via intermolecular interactions into a crystal (top) compared to the 1D chain chains in Series IIIb (bottom). Notice the slight skewedness of clusters in Series IIIa compared to the near-superimposed clusters in Series IIIb. ....	<b>103</b>
<b>Fig. III.9</b> A diagrammatic representation of supramolecular aggregation of 1:1 complex in (Series IIIa) via condensation and its transformation to a 1D chain (Series IIIb). ....	<b>103</b>
<b>Fig. III.10</b> Powder X-ray diffractograms for solids of Series IIIa (bottom) and Series IIIb (top) as compared to simulated pattern obtained from single crystal data. ....	<b>108</b>
<b>Fig. III.11</b> Rietveld refinement plot for solids reported in the work. The blue corresponds to the experimental data while the red represents calculated profile. ....	<b>111</b>
<b>Fig. III.12 (a-r)</b> FT-IR spectra of the solids reported. ....	<b>117</b>
<b>Fig. IV.1</b> Yellow crystals of Solid IVa were isolated when $\text{Na}_2\text{MoO}_4\cdot 2\text{H}_2\text{O}$ was used as the molybdate source. Solid IVa exhibits a 1D structure where a nine-coordinated $\{\text{Ln}(\text{DMF})_2(\text{H}_2\text{O})_5\}$ is coordinated on either sides of the cluster in a 1,4-manner. ....	<b>130</b>
<b>Fig. IV.2</b> Synthesis with $\text{K}_2\text{MoO}_4$ lead to the isolation of Series IVb. ....	<b>130</b>
<b>Fig. IV.3</b> A structural description of the series using $[\text{Tm}(\text{H}_2\text{O})_4(\text{DMF})_4][\text{Cr}(\text{OH})_6\text{Mo}_6\text{O}_{18}]\cdot x(\text{sol})$ as an example. (a) The cationic moiety	

[Tm(H<sub>2</sub>O)<sub>4</sub>(DMF)<sub>4</sub>]<sup>3+</sup>, (b) The anionic Anderson-Evans cluster, (c) View of the solid along bc-plane, (d) View of the solid along ab-plane, (e) A single layer along ab-plane. ....131

**Fig. IV.4** A comparison of Photoluminescent emission for Cr<sup>3+</sup> as well as Al<sup>3+</sup> analogues for solids of Series IVb. The chromium variants exhibited luminescence characteristics of Cr<sup>3+</sup> as well as respective Ln<sup>3+</sup>. ....136

**Fig. IV.5** Powder X-ray diffractograms for Series IVb (Cr) compared with the simulated pattern of CrTm. ....139

**Fig. IV.6** Powder X-ray diffractograms for Series IVb (Al) compared with the simulated pattern of AlEr. ....140

**Fig. IV.7** Rietveld Refinement plots for solids of Series IVb. ....142

**Fig. IV.8** FT-IR spectra for solids of Series IVb. ....144

**Fig. IV.9** TGA plots for selected solids of Series IVb. ....146

**Fig. V.1** The nine isomeric discrete octamolybdate {Mo<sub>8</sub>O<sub>26</sub>}<sup>4-</sup> species (left). Their abundance in the crystal structure database (top-right). The partially reduced  $\chi$ -isomer (bottom-right).154

**Fig. V.2** Structural landscape of lanthanide containing  $\beta$ -{Mo<sub>8</sub>O<sub>26</sub>}<sup>4-</sup> based solids isolated using our synthetic protocol in various solvents with two different Mo-sources (Na and K). Except Series V.c.2, all reactions led to solids that contained 1D chains of sodium coordinated with  $\beta$ -Mo<sub>8</sub>O<sub>26</sub> cluster. However, the way lanthanide solvated complex supramolecularly interacting with the 1D chain differed depending on the alkaline source and lanthanide cation. ....157

**Fig. V.3** The structural variations possible in octamolybdate based solids. ....158

**Fig. V.4** Structural variations in Series Va (solvent=DMSO, Mo-source=Na<sub>2</sub>MoO<sub>4</sub>.2H<sub>2</sub>O) along the lanthanide group. ....163

**Fig. V.5** Structural variations in Series Vc (solvent=DMA, Mo-source=Na<sub>2</sub>MoO<sub>4</sub>.2H<sub>2</sub>O) along the lanthanide group. ....165

<b>Fig. V.6</b> Structural variations in Series Vb (DMSO), Vd (DMA), and Ve (DMF) (Mo-source= $K_2MoO_4$ ). .....	<b>167</b>
<b>Fig. V.7</b> Powder X-ray diffractograms for selected solids of Series Va. ....	<b>182</b>
<b>Fig. V.8</b> Powder X-ray diffractograms for selected solids of Series Vb. ....	<b>183</b>
<b>Fig. V.9</b> Powder X-ray diffractograms for selected solids of Series Vc. ....	<b>184</b>
<b>Fig. V.10</b> Rietveld Refinement plots for selected solids of Series Va, Vb and Vc. ....	<b>188</b>
<b>Fig. V.11</b> FT-IR spectra for selected solids reported in this study. ....	<b>197</b>
<b>Fig. A.1</b> The crystal structure of solids of Series A1. The growth of 2D sheets is facilitated by the derivitization of a pair of lanthanide hydrate through terminal oxygen atoms on the cluster. ....	<b>209</b>
<b>Fig. A.2</b> A comparison of spatial arrangement of the cluster and the anion in Series A1 and Series IVb. The cluster and the cationic complex are held together via coordinate bond in the former and by H-bonds in the latter. ....	<b>210</b>
<b>Fig. A.3</b> The structure of solids in Series A2. A complex H-bonded network facilitates the growth of the 1D chains into a crystal. ....	<b>211</b>
<b>Fig. B.1</b> The addition of Imidazole to the synthetic scheme for Series IIa and IIb lead to the isolation of two concomitant solids. Solid B.1 contains a discrete anionic chain of the composition, $\{Mo_8O_{27}\}^{6-}$ that are derivatised with lanthanide hydrate. Solid B.2 contains a disordered Keggin cluster $\{Mo^{VI}_{12.5}O_{39}(OH)\}^{4-}$ and imidazolium cations assembled through H-bonding interactions. ....	<b>221</b>
<b>Fig. B.2</b> Structure of Solid B1. Each $\{Mo_8O_{27}\}^{6-}$ in the self-propagating 1D chain cluster is coordinated to six $\{Ln(H_2O)_4\}^{3+}$ , which in turn, is coordinated to three clusters, extending into a 2D sheets. The sheets are further stabilized via H-bonding interactions involving lattice water. ....	<b>222</b>

**Fig. B.3** Structure of Solid B2, containing the  $\{\text{Mo}_{12.5}\text{O}_{40}\}^{5-}$  cluster anions stabilized by imidazolium cations. ....224

## LIST OF TABLES

<b>Table I.1</b> Survey of Ln containing $\{\text{Cr}(\text{OH})_6\text{Mo}_6\text{O}_{18}\}^{3-}$ cluster based solids in Inorganic Crystal Structure Database (ICSD) (updated April 2022). .....	<b>17</b>
<b>Table I.2</b> Survey of Lanthanide based $\text{Cr}^{3+}$ -Anderson-Evans based solids in CSD 5.43 (June 2022). Highlighted solid reports luminescence from $\text{Dy}^{3+}$ and not from $\text{Cr}^{3+}$ ion. ....	<b>18</b>
<b>Table II.1</b> Crystal data and refinement details for all single crystals reported for the first time. ....	<b>46</b>
<b>Table II.2</b> Refined cell parameters for solids in Series IIa and Series IIb. ....	<b>48</b>
<b>Table II.3</b> Crystal structure and refinement parameters of reported solids that were resynthesized. ....	<b>50</b>
<b>Table II.4</b> Bond valence sum calculations for $\text{TbAl}_{23}$ and $\text{TmAl}_{27}$ . ....	<b>52</b>
<b>Table II.5</b> Excitation and emission spectra of optically active lanthanides along with corresponding energy levels of Sm, Eu, Tb and Dy. All the spectra are taken by a spectrofluorophotometer utilizing xenon lamp (see text). All assigned transitions (in parenthesis) are as per the reference [4]. ....	<b>66</b>
<b>Table II.6</b> Rietveld refined parameters of all unreported solids. ....	<b>72</b>
<b>Table II.7</b> FT-IR frequencies. ....	<b>79</b>
<b>Table II.8</b> Selected bond distances ( $\text{Å}$ ) and bond angles ( $^\circ$ ) of all the unreported solids prepared in the study. ....	<b>84</b>
<b>Table III.1</b> A CSD analysis of $\{\text{X}(\text{OH})_6\text{Mo}_6\text{O}_{18}\}^{3-}$ , with DMSO moiety present in the crystal structure. ....	<b>97</b>
<b>Table III.2</b> Crystal data and refinement details for all single crystals of Series IIIa and IIIb. ....	<b>103</b>
<b>Table III.3</b> Rietveld refined parameters for Series IIIa and IIIb. ....	<b>112</b>

<b>Table III.4</b> IR frequencies.....	<b>113</b>
<b>Table IV.1</b> A CSD analysis of $\{X(OH)_6Mo_6O_{18}\}^{3-}$ , where $X = Al^{3+}, Cr^{3+}$ , with the presence of DMF moiety in the crystal structure. Most of the structures, evidently, are tris alkoxy functionalized.....	<b>127</b>
<b>Table IV.2.</b> Crystal data and refinement details for single crystals for solids of Series IV..	<b>132</b>
<b>Table IV.3</b> Rietveld refinement parameters for solids of Series IVb.....	<b>143</b>
<b>Table IV.4</b> IR frequencies for solids of Series IVb.....	<b>145</b>
<b>Table V.1</b> Lanthanide based solids containing discrete octamolybdate isomers in crystal structure database.....	<b>155</b>
<b>Table V.2</b> Crystal data and refinement details for all single crystals for solids of Series Va. .....	<b>168</b>
<b>Table V.3</b> Crystal data and refinement details for single crystals of solids of Series Vb. ....	<b>174</b>
<b>Table V.4</b> Crystal data and refinement details for all single crystals for solids of Series Vc. .....	<b>177</b>
<b>Table V.5</b> Crystal data and refinement details for single crystals of solids of Series Vd and Ve. .....	<b>180</b>
<b>Table V.6</b> Rietveld refined parameters for selected solids of Series Va, Vb and Vc. ....	<b>189</b>
<b>Table V.7</b> FT-IR frequencies for solids of Series Va and Vb. ....	<b>198</b>
<b>Table V.8</b> FT-IR frequencies for solids of Series Vc.....	<b>200</b>
<b>Table A.1</b> Crystal data and refinement details for all single crystals for solids reported in Appendix A. ....	<b>212</b>
<b>Table B.1</b> Literature analysis of $Ln^{3+}$ based POMo architectures as reported in inorganic (ICSD) as well as organic/mixed (CCDC) media.....	<b>220</b>
<b>Table B.2</b> Literature analysis of “extended-octamolybdate”, $\{Mo_8O_{27}\}^{6-}$ , based solids in ICSD. .....	<b>223</b>

**Table B.3** Literature analysis of “isopoly-Keggin”  $\{Mo_{13}O_{40}\}^{n-}$ , cluster-based solids in CCDC. Highlighted solid is same as Solid B.2, however, attained using a different synthetic procedure. ....**224**

**Table B.4** Crystal data and refinement details for solid B1 and B2. ....**225**

**Table VI.1** A compendium of structural variety isolated in this work with synthetic changes incurred. ....**235**

## List of abbreviations

CP	coordination polymer
CSD	Crystal Structural Database
CCDC	Cambridge crystallographic Data Centre
DMA	Dimethyl acetamide
DMF	Dimethyl formamide
DMSO	Dimethyl sulfoxide
EDTA	ethylenediaminetetraacetic acid
ICSD	Inorganic Crystal Structure Database
MOF	metal-organic framework
<i>ox</i>	oxalato
POM	Polyoxometalate
POMo	Polyoxomolybdate
<i>pzc species</i>	<i>point zero charged</i>
TBA	tetrabutylammonium
TMA	tetramethylammonium